Journal of Power Sources 226 (2013) 249–255

Contents lists available at SciVerse ScienceDirect

Journal of Power Sources

journal homepage: www.elsevier.com/locate/jpowsour

Design of a new lithium ion battery test cell for *in-situ* neutron diffraction measurements

Matthew Roberts [a,*], Jordi Jacas Biendicho [b,c], Stephen Hull [b], Premysl Beran [d], Torbjörn Gustafsson [a], Gunnar Svensson [c], Kristina Edström [a]

[a] Department of Chemistry – Ångström Laboratory, Uppsala University, Box 538, SE-751 21 Uppsala, Sweden
[b] The ISIS Facility, STFC Rutherford Appleton Laboratory, UK
[c] Department of Material and Environmental Chemistry, Stockholm University, Sweden
[d] Nuclear Physics Institute ASCR, Rez, Czech Republic

HIGHLIGHTS

- A new cell design for *in situ* neutron diffraction measurements of lithium ion batteries.
- Cell components are compared and a combination to provide optimal electrochemical and diffraction measurements is identified.
- Structural changes during charge and discharge of a LiFePO4 cathode are monitored.
- Patterns were refined to obtain lattice parameters and atomic positions.

GRAPHICAL ABSTRACT

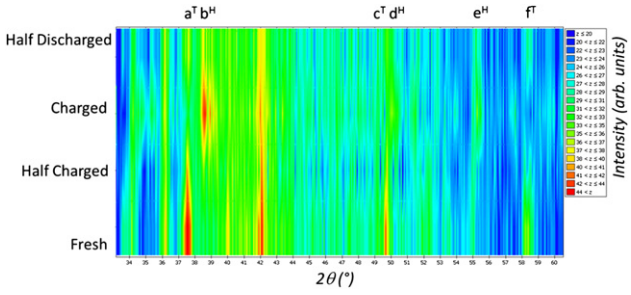

ARTICLE INFO

Article history:
Received 2 August 2012
Received in revised form
9 October 2012
Accepted 29 October 2012
Available online 8 November 2012

Keywords:
Neutron
Lithium
$LiFePO_4$
Diffraction
In situ

ABSTRACT

This paper introduces a new cell design for the construction of lithium ion batteries with conventional electrochemical performance whilst allowing *in situ* neutron diffraction measurement. A cell comprising of a wound cathode, electrolyte and anode stack has been prepared. The conventional hydrogen-containing components of the cell have been replaced by hydrogen-free equivalents. The electrodes are fabricated using a PTFE binder, the electrolyte consists of deuterated solvents which are supported in a quartz glass fibre separator. Typical battery performance is reported using the hydrogen-free components with a specific capacity of 140 mA h g^{-1} being observed for $LiFePO_4$ at a rate of 0.2 C. Neutron diffraction patterns of full cells were recorded with phase change reactions monitored. When aluminium packaging was used a better signal to noise ratio was obtained. The obtained atomic positions and lattice parameters for all cells investigated were found to be consistent with parameters refined from the diffraction pattern of a powder of the pure electrode material. This paper highlights the pertinent points in designing cells for these measurements and addresses some of the problems.

1. Introduction

Lithium ion batteries have become an important part of the modern world, powering the portable electronics revolution [1,2]. These systems generally work using the insertion and removal of lithium ions into host materials which drives an electrical current through an external circuit. During operation of the battery

* Corresponding author. Tel.: +46 (0) 18 4713700; fax: +46 18 4713701.
E-mail address: matthew.roberts@kemi.uu.se (M. Roberts).

0378-7753/$ – see front matter © 2012 Elsevier B.V. All rights reserved.
http://dx.doi.org/10.1016/j.jpowsour.2012.10.085

significant structural changes occur in the electrode materials which are extremely important in understanding the electrochemical observations. This knowledge can reveal the causes of cell failure and provide new directions of research to improve material performance. The collection of *in situ* diffraction patterns during electrochemical testing of such batteries is an elegant approach to obtain this information.

In situ diffraction methods have been demonstrated extensively within the literature using X-ray scattering [3–5] and to a lesser extent with neutrons [6–13]. *In situ* X-ray diffraction measurements are more commonly used because the equipment required is present in most laboratories or at synchrotron facilities and conventional cell designs and components can be readily modified. However, the following list identifies three important advantages which can be achieved using neutrons:

- The determination of the locations and site occupancies of light elements such as Li in the presence of heavier species is possible.
- The differences between transition metal elements (Fe, Ni, Co, Mn) of similar mass weight can be resolved.
- The penetration depth is large, so an average pattern can be recorded for cells as large as those used within a conventional laptop.

The difference between X-ray and neutron techniques is highlighted in Fig. 1 where the diffraction pattern of $LiFePO_4$ using both methods is shown (calculated from database structural values using identical wavelengths for both). Whilst the peak positions are identical, the peak intensities are significantly different due to the different scattering of the two types of radiation from the individual elements.

In neutron diffraction, neutrons interact directly with the nucleus of the atom, and the contribution to the diffracted intensity is different for each isotope. This results in the scattering length of each atom for neutrons not being dependent on the atomic number and, therefore, means that the technique is very appropriate to obtain accurate positions of elements commonly found in the battery such as Li ($b = -1.9$ fm) and D ($b = 6.67$ fm) or to distinguish between near neighbour elements in the periodic table such as a Mn ($b = -3.73$ fm), Fe ($b = 9.45$ fm) and Co ($b = 2.49$ fm). At the same time, the diffracted intensity shows less variation with wavelength and scattering angle compared to X-rays (see degradation of intensity for X-ray pattern in Fig. 1).

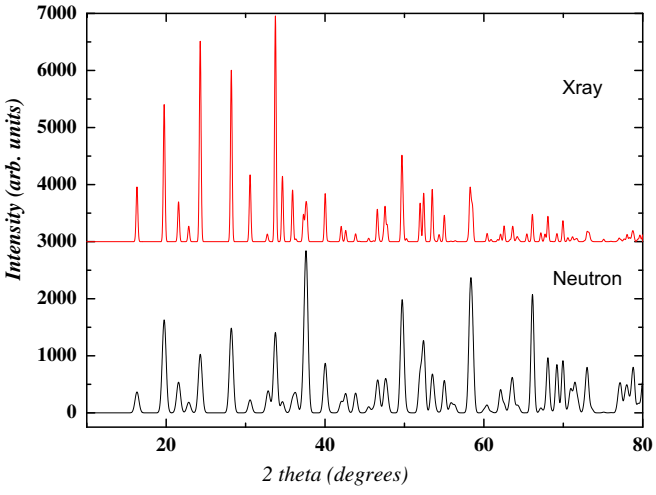

Fig. 1. Calculated X-Ray and neutron diffraction patterns of $LiFePO_4$ taking a wavelength of 1.46 Å based on structural information obtained form Andersson et al. [3].

However, a significant disadvantage when making neutron diffraction measurements is the very high incoherent scattering cross section of hydrogen which in many cases (especially in *in situ* battery cells) adds a significant background to the diffraction pattern and may lead to a complete masking of the Bragg reflections. For this reason, we must aim for H-free cells.

The first report of an *in situ* neutron diffraction measurement of a lithium ion battery was by our research group in 1998 [8]. This was used effectively to study the charge and discharge reaction of $LiMn_2O_4$ [7]. However, this cell suffered from a problem in that the thick cathode layer meant that only very slow charge and discharge rates (<C/50) could be used to obtain reasonable electrochemical cycling data. This limited the electrochemical test to unrealistically slow charge and discharge rates and no kinetic information could be extracted out of the diffraction experiments. Also, from a practical point of view, charging at these slow rates does not well utilise the limited times available at neutron diffraction facilities. In 2008 Rosciano et al. [11] presented a new cell design. This design was later used to study $LiNiO_2$, $LiNi_{1/3}Co_{1/3}Mn_{1/3}O_2$ and $Li_4Ti_5O_{12}$ [9]. This is a novel design which exposes only the cathode to the neutron beam, resulting in simpler diffraction patterns. However, the cathode electrode is again very thick (~5 mm) leading to similar problems to those observed in our own work.

Recent publications in 2010 by Sharma et al. [13] and Rodriguez et al. [10] have demonstrated the use of commercial Li-ion batteries for neutron diffraction studies. These experiments have the advantage of being extremely industrially relevant and should operate with excellent electrochemical behaviour. However, the presence of large amounts of hydrogen in the cell have led to significant interference in the recorded patterns from high backgrounds. Recently work by Sharma et al. [12,14–17] has improved their technique by reducing the amount of hydrogen within the battery and has been used to study $LiFePO_4$, MoS_2 and $Li_5Ti_4O_{12}$.

This paper aims to show a new approach to fabricating a battery for *in situ* collection of diffraction patterns and demonstrate a proof of concept experiment studying a $LiFePO_4$ electrode under charge and discharge.

2. Experimental

2.1. Electrode fabrication

Conventional and hydrogen free electrodes were prepared:

- Conventional: $LiFePO_4$ electrodes were made with a 75:15:10 wt.% ratio of $LiFePO_4$, carbon black and PVdF binder (Kynar) respectively, these components were suspended in *N*-Methyl-2-pyrrolidone (NMP) to form an ink which was spread across a piece of aluminium foil. The solvent was removed to form a solid layer adhered to the foil. This was then cut into appropriate sizes for testing.
- Hydrogen free: The cathode films contained 75 wt.% of $LiFePO_4$, 15 wt.% of Carbon (Super P) and 10 wt.% polytetrafluoroethylene (PTFE, Type: 6C–N, DuPont) binder. These components were combined dry using a pestle and mortar. The materials were pressed into a lump and rolled using a mill (Minimill, Durston) into a film approximately 60 μm thick. The resulting films were of random shapes with an area of a few centimetres each. These pieces were then tessellated onto pieces of aluminium mesh (TWP, 200 mesh) with the required electrode dimension such that little of the mesh beneath was visible. This was then pressed again using a rolling mill to adhere the film to the mesh. The mesh was then turned over and the process repeated so that both sides were coated in active material.

2.2. Electrolyte

Three different electrolytes were used in these experiments:

- Conventional: A commercial electrolyte containing 1 M $LiPF_6$ in a 1:1 mixture of Ethylene Carbonate (EC)/diethyl carbonate (DEC) supplied by Purelyte.
- Deuterated: In house prepared 1 M $LiPF_6$ in a 1:4 mixture of Ethylene Carbonate (EC)/dimethyl carbonate (DEC). The EC and PC were both supplied in the deuterated form from Qmx Laboratories. The EC and PC were first combined and left with molecular sieve for 48 h to reduce the levels of water impurities (Karl Fisher measurements showed that the water content was reduced to below 10 ppm).
- Flourinated: In house prepared 1 M $LiPF_6$ in methyldifluoroacetate (MFA, supplied by DAIKIN Chemical) which had been dried with molecular sieve for 48 h as above. (Karl Fisher measurements indicated similar water content was achieved as for the deuterated electrolytes).

2.3. Full cell construction

The battery stack is either housed in a quartz or aluminium tube as shown in Fig. 2b and c sealed at both ends using Swagelock joints. A cylindrical cell design was chosen to ensure that a constant pathlength and therefore a constant absorption was experienced by all neutrons exiting at all angles from the cell. These joints have PTFE ferrels so as to electronically insulate the central tube from each end piece. The ends of the Swagelock tubes are sealed using metal current collectors, one of which is copper and the other aluminium. These current collectors are metallic cylinders with an aperture where wires from the electrode stack can be inserted and contacted to using a grub screw. In the case where all conventional components were used, established "coffee bag" packaging and vacuum sealing technique was implemented [3]. Inside the main tube the wound cell is inserted as shown schematically in Fig. 2a. The electrode, separator (pre-soaked in electrolyte), lithium foil and a further piece of separator are placed on top of one another to form a stack which is rolled into a coil as shown in the top view cell interior schematic. This process can be thought of similar to how one prepares the cakes "swiss roll" or "chocolate log". By using this approach thin electrodes (<70 μm) can be used to obtain high quality electrochemical performance and large sample masses (1–3 g) can be used to ensure high quality diffraction data. The large quantities of sample will ensure large count rates and short collection times. The Swagelok ends are then closed and the cell is ready for testing. This whole construction process was completed in an argon filled glove box (H_2O, $O_2 < 1$ ppm; Unilab from MBraun). Table 1 summarises the composition of the 4 cell designs prepared. Also shown in Table 1 is a comparison of the percentage of sample and hydrogen in the four battery configurations. The values were calculate based on approximations of the battery compositions and are not exact, but give a guide to the expected quantities.

Cell 1 was built using an all conventional construction, including the following hydrogen containing components; PVdF ($(C_2\mathbf{H_2}F_2)_n$), EC ($C_3\mathbf{H_4}O_3$), DEC ($C_5\mathbf{H_{10}}O_3$), and Polypropylene ($(C_3\mathbf{H_6})_n$). These contribute to substantial levels of hydrogen within the cell (indicated in Table 1) which will result in large incoherent scattering reducing the likelihood of obtaining high quality diffraction data. In Cells 2, 3 and 4 we used alternative components to reduce the amount of hydrogen. The PVdF binder was replaced by PTFE ($(C_2F_4)_n$). The EC and DEC electrolytes are replaced by deuterated equivalents in Cells 2 and 4. In Cell 3 MFA ($F_2C\mathbf{H}CO_2C\mathbf{H_3}$) electrolyte was used to reduce the hydrogen content.

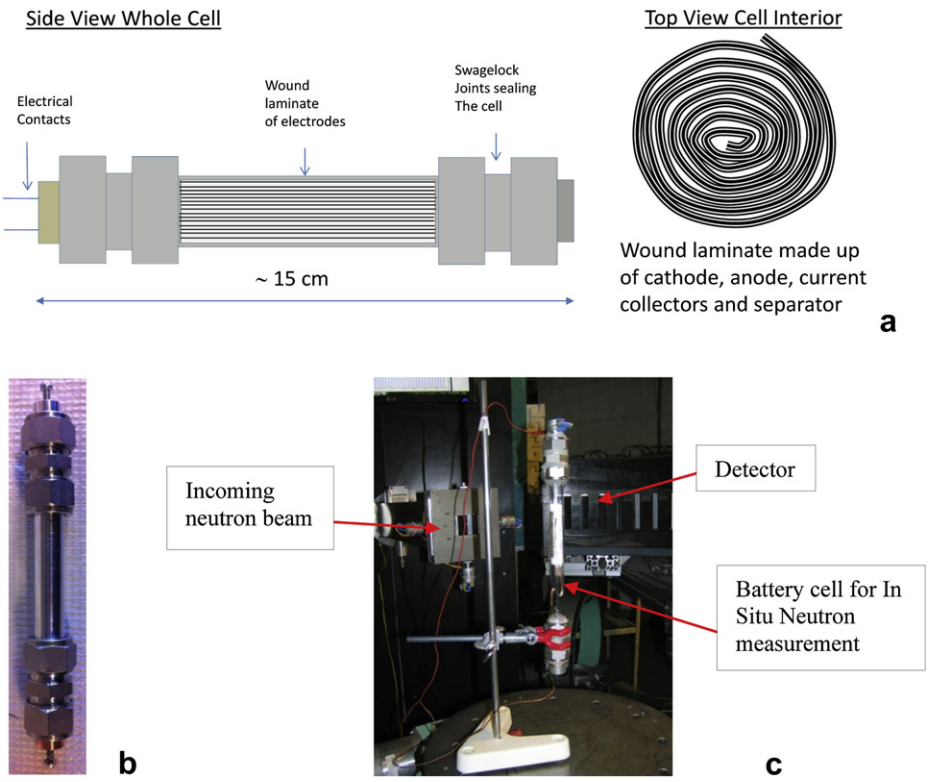

Fig. 2. Images of the battery cell for *in situ* neutron diffraction measurement. a) A schematic of the battery cell. b) A photo of the diffraction setup sealed in aluminium tube (Cell 4). c) A photo of the cell design and placement on the diffraction instrument goniometer (Cell 2).

Table 1
Summary of the cells prepared for testing and the approximate sample mass and hydrogen percentages for the various designs.

Cell type	Cathode	Separator and electrolyte	Anode	Packaging	Mass of $LiFePO_4$	Mass % $LiFePO_4$	Mass % H	Atomic % $LiFePO_4$	Atomic % H
Cell 1	$LiFePO_4$, Carbon, PVDF binder on Al foil	Polypropylene soaked in conventional electrolyte	Lithium metal	Polypropylene/ Aluminium coffee bag	~1 g	~13	~4.5	~5.4	~40
Cell 2	$LiFePO_4$, Carbon, PTFE binder on Al Mesh	Quartz glass fibre soaked in deuterated electrolyte	Lithium metal	Quartz glass tube	~1 g	~13	~0	~7	~0
Cell 3	$LiFePO_4$, Carbon, PTFE binder on Al Mesh	Quartz glass fibre soaked in flourinated electrolyte	Lithium metal	Quartz glass tube	~1 g	~13	~1.5	~7	~24
Cell 4	$LiFePO_4$, Carbon, PTFE binder on Al Mesh	Quartz glass fibre soaked in deuterated electrolyte	Lithium metal	Aluminium tube	~1 g	~13	~0	~7	~0

2.4. Small pouch cell testing

Some electrochemical testing was also performed using a standard "coffee bag" or pouch cell described previously [3]. Cells were assembled in an argon-filled glove box (H_2O, $O_2 < 1$ ppm; Unilab from MBraun). Lithium foil was used both as the counter and reference electrode in all cases. The cells were cycled galvanostatically at a range of different currents between 2.0 and 4.2 V vs. Li using a Digatron Battery cycler.

2.5. Diffraction setup

The battery cells were mounted on the sample position of the neutron powder diffractometer MEREDIT at the Nuclear Physics Institute ASCR in Rez (Czech Republic) as shown on the Fig. 2c. All diffraction patterns were collected at room temperature using neutrons with wavelength of 1.46 Å extracted from the primary beam by mosaic copper monochromator (reflection 220). Angular range of patterns was between 4 and 144° 2θ with step of 0.08° 2θ and step delay controlled by monitor (constant neutron flux on sample for each step). Charging and discharging of the battery cell was performed between the collection of diffraction patterns at a rate of C/3 using a biologic SP240 potentiostat without removing the cell from the instrument.

3. Results and discussion

3.1. Electrochemical performance

The electrochemical battery performance of cells constructed with the new components is compared with a standard battery in Fig. 3. The cells were built in the same formulations as Cells 1, 2 and 3, but in a standard "coffee bag" cell to reduce wastage of the expensive deuterated and fluorinated components. A flat charge and discharge plateau occurring around 3.45 V vs. Li consistent with $LiFePO_4$ is seen in all three cases [18,19]. Full discharge capacity of between 130 and 140 mA h g^{-1} is seen for all three cells. The cells were also tested at higher rates with the standard and hydrogen free batteries exhibiting a very similar performance with ~100 mA h g^{-1} observed at a rate of 5 C. The cell constructed using fluorinated electrolyte showed only 80 mA h g^{-1} at 5 C which we speculate is due to a reduction in the ionic conductivity. This demonstrates that we can achieve the expected electrochemical behaviour using the reduced hydrogen components.

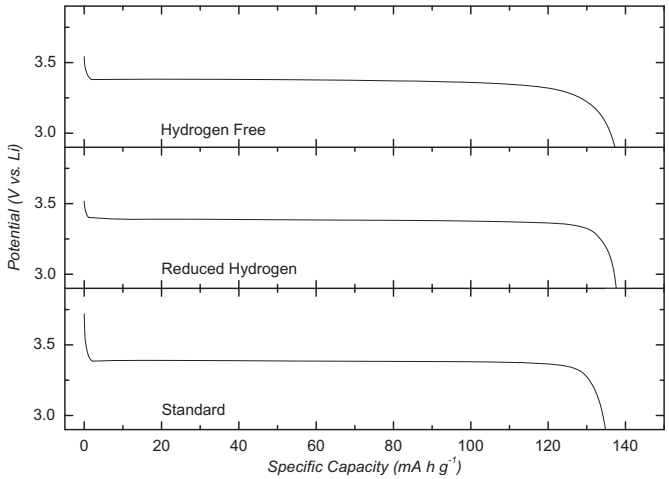

Fig. 3. Charge and discharge cycles at C/5 of $LiFePO_4$ vs. Li for batteries fabricated using hydrogen free, reduced hydrogen and conventional components.

3.2. Neutron diffraction of pure $LiFePO_4$ powder

The neutron diffraction pattern of the $LiFePO_4$ powder used in the battery was first acquired to provide a baseline for comparison with *in situ* measurements. The measured and calculated diffraction patterns are shown in Fig. 4 along with the difference line indicating a good fit. The atomic positions obtained as a result of this refinement are shown in Table 2. The values correspond well with those previously reported for this material within the literature [3].

3.3. In situ neutron diffraction of $LiFePO_4$ in a battery

The neutron diffraction pattern of Cell 1 which contained all conventional components was recorded. There was a large background on the pattern and no Bragg peaks could be resolved as

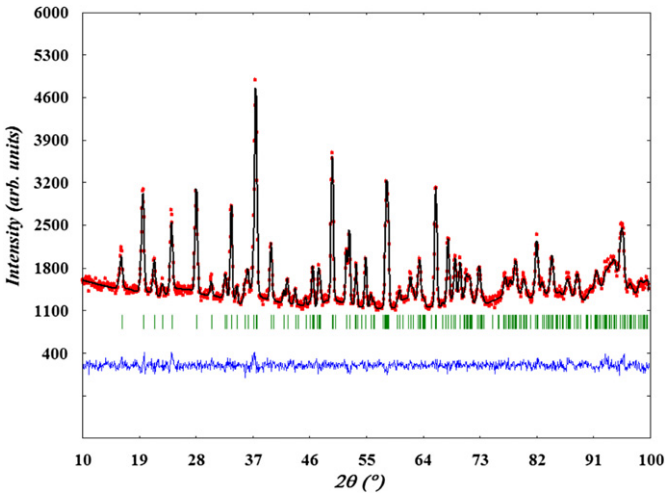

Fig. 4. Measured (points) and calculated (line) diffraction patterns of pure $LiFePO_4$ powder sealed within a Vanadium can. Small ticks represent Bragg positions and the lower line difference of measured and calculated patterns is shown.

Table 2
Atomic parameters obtained from Rietveld refinement of neutron powder diffraction data of $LiFePO_4$ powder (Diffraction pattern displayed in Fig. 4).

Atom	x	y	z	$100 \times U_{iso}$ (Å^2)
Li	0	0	0	2.85(48)
Fe	0.2822(3)	0.25	0.9704(10)	0.82(7)
P	0.0949(6)	0.25	0.4181(13)	0.43(12)
O	0.0961(7)	0.25	0.7477(14)	1.01(12)
O	0.4570(5)	0.25	0.2011(13)	0.62(13)
O	0.1651(4)	0.0499(7)	0.2819(8)	0.50(7)

S.G. Pnma, $a = 10.3333(3)$ Å $b = 6.0095(2)$ Å $c = 4.6949(1)$ Å.
$\chi^2 = 1.77$, $R_b = 2.66\%$.

Table 3
Atomic parameters obtained for $LiFePO_4$ from Rietveld refinement of neutron powder diffraction data recorded for Cell 2 in the discharged state (Diffraction pattern displayed in Fig. 5).

Atom	x	y	z	$100 \times U_{iso}$ (Å^2)
Li	0	0	0	0.6
Fe	0.2803(14)	0.25	1.0078(52)	0.6
P	0.0974(8)	0.25	0.4081(17)	0.6
O	0.0974(20)	0.25	0.7279(19)	0.6
O	0.4596(11)	0.25	0.1965(50)	0.6
O	0.1632(18)	0.0571(22)	0.2643(38)	0.6

S.G. Pnma, $a = 10.3401(14)$ Å $b = 6.0078(8)$ Å $c = 4.6937(6)$ Å.
Final $\chi^2 = 1.52$, $R_b = 1.11\%$.

expected due to the hydrogen content. We then recorded diffraction data for Cell 2 which contained all hydrogen free components housed within a quartz tube. A neutron diffraction pattern of the middle section of the cell containing the wound battery was recorded over 15 h to obtain improved statistics. Measured and calculated neutron diffraction patterns of the multiphase system present in Cell 2 are shown in Fig. 5. A significant background is seen as a result of the thick (1 mm) amorphous quartz glass housing. However, on top of this broad background the reflections from $LiFePO_4$, Al and Li can be resolved. The results of the multiphase Rietveld refinement is summarised in Table 3. Refinement of the thermal parameters lead to very large errors in sigmas and, therefore, the sigma values were fixed to 0.6 (Å^2). Close examination of the data shows that only a few of the most intense $LiFePO_4$ peaks are significant enough to be useful in the refinement. However, refined lattice parameter and atomic positions are in good agreement with those refined for the pure $LiFePO_4$ powder.

A charging current (at a rate of C/3) was then applied to the cell; an initial voltage plateau at 3.6 V was seen until the cell had been charged to approximately 50% of full charge as shown in Fig. 6b. A further diffraction pattern was collected at this point. We then charged the cell fully using a constant current (C/3) constant voltage (potential hold at 4.2 V) and recorded a third pattern before finally discharging (C/3) the cell to 50% of full charge and recording a final pattern. The changes in the diffraction pattern as a function of the state of charge are shown in the colour map in Fig. 6a along with the voltage capacity profile recorded during this study. The most intense Bragg reflection for $LiFePO_4$ is at approximately 37.5° (a^T). The peak intensity of this gradually drops to background levels as the battery is charged and then on discharge reappears as

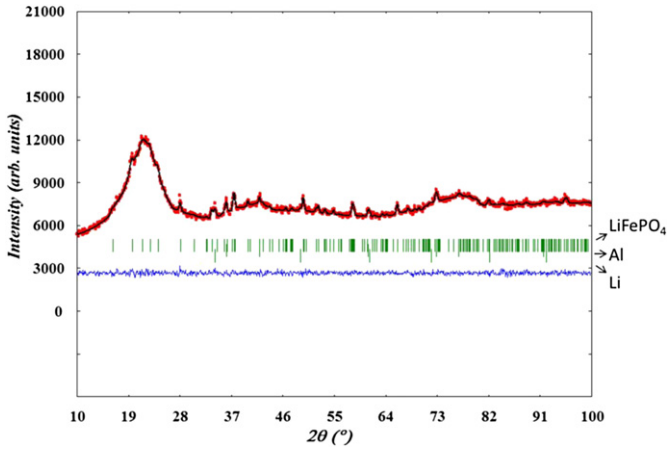

Fig. 5. Measured and refined neutron diffraction pattern of Cell 2 containing a full as constructed $LiFePO_4$ vs. Li cell contained within a quartz tube. Small ticks represent Bragg positions and the lower line difference of measured and calculated patterns is shown.

expected (this is also true for the other intense peaks of $LiFePO_4$ at 49.7 (c^T) and 58.3 (f^T) degrees). The inverse behaviour is seen for the intense peaks of $FePO_4$ at 38.5(b^H), 50.1 (d^H) and 55 (e^H) degrees. This is indicative of the growth of the $FePO_4$ phase on charging and gradual disappearance on discharging. This is consistent with *in situ* X-ray results that have been published elsewhere [3] and shows that the cell design and new components allow for the cell to operate via the expected mechanism. In the electrochemical data (Fig. 6b) an unusual feature is seen on the discharge which was not seen in our small scale testing done in pouch cells. We believe this may be a result of redox reaction of an impurity affecting the discharge voltage. However, the behaviour is still reasonably consistent with that typically observed for $LiFePO_4$. This is an important result as it indicates that both conventional electrochemical and structural behaviour can be expected from the battery materials assembled into a cell in this manner.

Refinements of the diffraction patterns recorded of the cell at various states of charge were also performed; a summary of these refinements are presented in Table 4 and Table 5. Refinements of the fresh, charged and half discharged cells were all successful and gave reasonable lattice parameters and phase fractions. Although we also recorded a pattern for the cell in the half charged state refinement was not possible as only half the collection time was used and the data was of insufficient quality (therefore, we only present this result in the colour map shown in Fig. 6a). The refined phase fractions of $LiFePO_4$, $FePO_4$, Li and Al for the charged, discharged and half discharged are shown in Fig. 7. These results show that the phase fractions of Li and Al stay almost constant throughout charge as expected. The phase fractions of $LiFePO_4$ and $FePO_4$ change as expected during charging with ~40% $LiFePO_4$ seen in the freshly prepared battery. In the half discharged case around 20% of each phase is observed consistent with the composition expected from the electrochemistry. In the fully charged battery ~40% $FePO_4$ is seen and no $LiFePO_4$ even though it was only possible to charge the battery to 90% of its theoretical capacity (which is a common result for this material) [3].

The neutron diffraction pattern of Cell 3, where the deuterated electrolytes were replaced with a fluorinated equivalent, was then recorded. This pattern was extremely poor and for the same collection time as used for Cell 2, no peaks were observed. This again proved that batteries containing high proportions of hydrogen are not suitable for the neutron diffraction. Whilst on a high intensity source we may be able to extract some useful data, it is believed that if possible the use of deuterated solvents is the best solution.

To reduce the high background levels caused by the quartz tube we replaced it with an aluminium equivalent (Cell 4). The quartz was originally selected as our previous work in this field had focused on its use for the cell packaging [8]. Aluminium was felt to be a logical alternative due to it ubiquitous use in battery construction and low cost. The aluminium will not result in significant levels of incoherent scattering which means that the

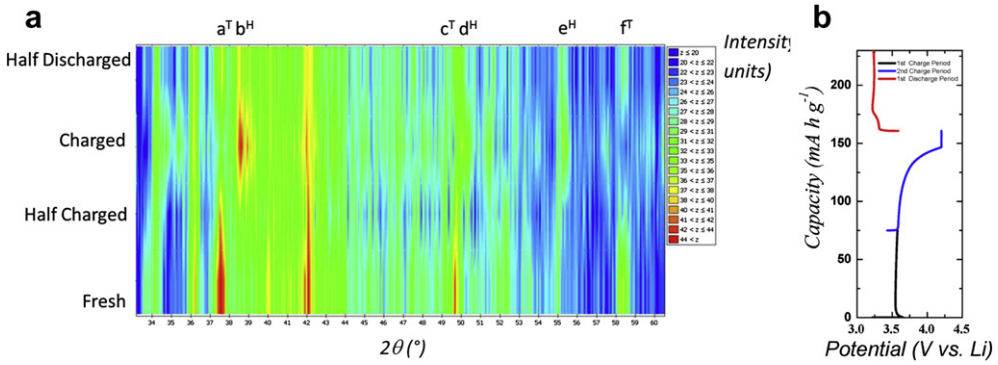

Fig. 6. Summary of diffraction and electrochemistry results for Cell 2. a) Colour map showing the diffraction intensity vs. the 2 theta angle as a function of the state of charge within the cell. b) Electrochemical behaviour recorded during *in situ* measurement (gravimetric capacity shown is cumulative passed from both charge and discharge currents). (For interpretation of the references to colour in this figure legend, the reader is referred to the web version of this article.)

Table 4
Atomic parameters obtained for $LiFePO_4$ and $FePO_4$ from Rietveld refinement of neutron powder diffraction data recorded for Cell 2 in the half discharged state.

Atom	*x*	*y*	*z*	$100 \times U_{iso}$ (Å^2)
$LiFePO_4$				
Li	0	0	0	0.6
Fe	0.2845(45)	0.25	0.9966(122)	0.6
P	0.1065(80)	0.25	0.4186(167)	0.6
O	0.0930(78)	0.25	0.7013(164)	0.6
O	0.4485(77)	0.25	0.1911(186)	0.6
O	0.1669(124)	0.0619(166)	0.2626(224)	0.6
$FePO_4$				
Fe	0.2762(42)	0.25	0.9434(86)	0.6
P	0.0911(68)	0.25	0.4161(179)	0.6
O	0.1097(58)	0.25	0.7264(136)	0.6
O	0.4444(77)	0.25	0.1574(130)	0.6
O	0.1714(91)	0.0574(138)	0.2479(210)	0.6

For $LiFePO_4$: S.G. Pnma, $a = 10.3337(43)$ Å $b = 5.9984(23)$ Å $c = 4.6869(19)$ Å.
For $FePO_4$: S.G. Pnma, $a = 9.8348(36)$ Å $b = 5.7897(19)$ Å $c = 4.7840(17)$ Å.
Final $\chi^2 = 1.57$, $R_b = 1.45\%$.

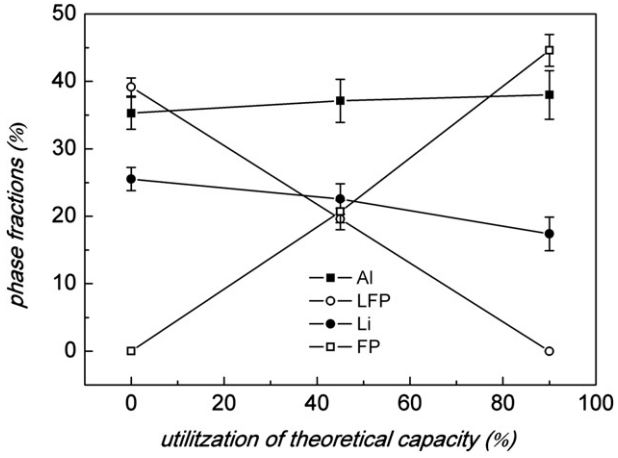

Fig. 7. The relative amounts of the phases $LiFePO_4$, Li, Al, $FePO_4$ calculated from refinements plotted as a function of charge passed.

signal to noise ratio for the sample reflections should be much improved, though Bragg peaks of aluminium will be observed. Cell 4 was constructed using this concept and the Rietveld refinement of the diffraction pattern is shown in Fig. 8. In comparison with Cell 2 we observed the same phases and additional reflections from PTFE. The PTFE was also present in Cell 2 as it was used as a binder, however, in this cell we have a higher content as it was also used as a final layer of insulation to separate the lithium from the aluminium casing. A good agreement between the calculated and experimental patterns was obtained with good fits easily observed even for peaks with a low intensity. The difference line shows several intensity mismatches on the aluminium reflections. The explanation for this is because the aluminium tube had a very strong complex (multi-directional) texture which is very difficult to refine. However, the Bragg reflections of the aluminium do not significantly influence or cover the important reflections of the other phases in the cell. The results from the refinement are shown in Table 6. The lattice parameters and atomic positions are in good agreement with those seen for the pure powder material. However,

Table 5
Atomic parameters obtained for $FePO_4$ from Rietveld refinement of neutron powder diffraction data recorded for Cell 2 in the fully charged state.

Atom	*x*	*y*	*z*	$100 \times U_{iso}$ (Å^2)
Fe	0.2772(23)	0.25	0.9553(43)	0.6
P	0.0955(39)	0.25	0.4163(93)	0.6
O	0.1148(34)	0.25	0.7151(70)	0.6
O	0.4401(41)	0.25	0.1782(72)	0.6
O	0.1677(59)	0.0352(87)	0.2672(109)	0.6

S.G. Pnma, $a = 9.8228(19)$ Å $b = 5.7856(10)$ Å $c = 4.7848(10)$ Å.
Final $\chi^2 = 1.77$, $R_b = 1.24\%$.

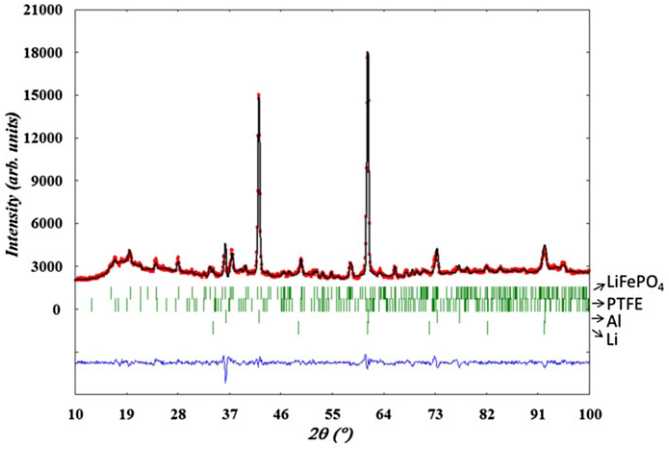

Fig. 8. Measured (points) and calculated (line) neutron diffraction pattern of Cell 4 as constructed full $LiFePO_4$ vs. Li cell sealed within an Aluminium tube. Small ticks represent Bragg reflections for each phase and the lower line is a difference pattern.

Table 6
Atomic parameters obtained for $LiFePO_4$ from Rietveld refinement of neutron powder diffraction data recorded for Cell 4 in the discharged state.

Atom	x	y	z	$100 \times U_{iso}$ (Å^2)
Li	0	0	0	2.85
Fe	0.2848(19)	0.25	0.9760(54)	0.82
P	0.0952(9)	0.25	0.4135(18)	0.43
O	0.0847(35)	0.25	0.7345(21)	1.01
O	0.4601(16)	0.25	0.2055(79)	0.62
O	0.1653(23)	0.0453(26)	0.3013(42)	0.50

S.G. Pnma, $a = 10.3351(16)$ Å $b = 6.0088(9)$ Å $c = 4.6968(7)$ Å.
$\chi^2 = 7.19$, $R_b = 3.23\%$.

thermal parameters were not added to the refinement due to their large error sigmas. Much to our disappointment an instrumental issue occurred with our potentiostat during this trip to the diffraction facility and we were unable to demonstrate any *in situ* cycling of Cell 4. However, since only the housing has been changed the results should be identical.

4. Conclusions

We conclude that cells with good electrochemical performance can be prepared using hydrogen free components. The collected data from the cell contained within quartz could be used to monitor the phase change reaction occurring at the electrode and to obtain lattice parameters. To reduce the signal from the amorphous quartz tube we also try to use aluminium tube as a sealing material. These patterns could be used to refine lattice parameters and atomic coordinates with values comparable to those seen for the *ex situ* measurement of the same material.

5. Future work

Several further improvements will be made to the cell design; we will reduce the thickness of the aluminium tube walls used to construct the cell, improve the electrolyte drying procedures and increase the size of the cell to increase the sample mass. The cell will then be used for scientific studies on materials performance using both the MEREDIT (reactor source) at the *Nuclear Physics Institute ASCR* and the POLARIS (spallation source) instrument at ISIS. POLARIS is a high intense, medium resolution powder diffractometer. The combination of the intense neutron flux with a large detector solid angle will allow collecting the *in situ* data from our electrochemical cell with short counting rates and, therefore, characterising electrode materials at high rates of charge and discharge.

Acknowledgements

The authors would like to extend special thanks to Anders Lund, Håkan Rundlöf and Henrik Eriksson for their assistance in experimental setup and cell manufacture. This work has been funded by the Swedish Research Council (VR) and Prof. Sten Eriksson, Chalmers, under the contract 822-2009-5870, StandUp for Energy and by Uppsala University. P.B. wants to thank the support from the CANAM infrastructure. We would also like to extend our sincere thanks to all the staff at the *Nuclear Physics Institute ASCR* for their kind assistance with these measurements.

References

[1] M. Roberts, P. Johns, J. Owen, D. Brandell, K. Edstrom, G. El Enany, C. Guery, D. Golodnitsky, M. Lacey, C. Lecoeur, H. Mazor, E. Peled, E. Perre, M.M. Shaijumon, P. Simon, P.-L. Taberna, Journal of Materials Chemistry 21 (2011) 9876.
[2] J.M. Tarascon, M. Armand, Nature 414 (2001) 359–367.
[3] A.S. Andersson, B. Kalska, L. Haggstrom, J.O. Thomas, Solid State Ionics 130 (2000) 41–52.
[4] M. Morcrette, Y. Chabre, G. Vaughan, G. Amatucci, J.B. Leriche, S. Patoux, C. Masquelier, J.M. Tarascon, Electrochimica Acta 47 (2002) 3137–3149.
[5] J.N. Reimers, J.R. Dahn, Journal of The Electrochemical Society 139 (1992) 2091–2097.
[6] H. Berg, H. Rundlöv, J.O. Thomas, Solid State Ionics 144 (2001) 65–69.
[7] H. Berg, J.O. Thomas, Solid State Ionics 126 (1999) 227–234.
[8] O. Bergstom, A.M. Andersson, K. Edstrom, T. Gustafsson, Journal of Applied Crystallography 31 (1998) 823–825.
[9] J.-F. Colin, V. Godbole, P. Novák, Electrochemistry Communications 12 (2010) 804–807.
[10] M.A. Rodriguez, D. Ingersoll, S.C. Vogel, D.J. Williams, Electrochemical and Solid-state Letters 7 (2004) A8–A10.
[11] F. Rosciano, M. Holzapfel, W. Scheifele, P. Novak, Journal of Applied Crystallography 41 (2008) 690–694.
[12] N. Sharma, G. Du, A.J. Studer, Z. Guo, V.K. Peterson, Solid State Ionics 199–200 (2011) 37–43.
[13] N. Sharma, V.K. Peterson, M.M. Elcombe, M. Avdeev, A.J. Studer, N. Blagojevic, R. Yusoff, N. Kamarulzaman, Journal of Power Sources 195 (2010) 8258–8266.
[14] N. Sharma, M.V. Reddy, G. Du, S. Adams, B.V.R. Chowdari, Z. Guo, V.K. Peterson, The Journal of Physical Chemistry C 115 (2011) 21473–21480.
[15] N. Sharma, V. Peterson, Journal of Solid State Electrochemistry 16 (2012) 1849–1856.
[16] N. Sharma, X. Guo, G. Du, Z. Guo, J. Wang, Z. Wang, V.K. Peterson, Journal of the American Chemical Society 134 (2012) 7867–7873.
[17] G. Du, N. Sharma, V.K. Peterson, J.A. Kimpton, D. Jia, Z. Guo, Advanced Functional Materials 21 (2011) 3990–3997.
[18] A.K. Padhi, K.S. Nanjundaswamy, J.B. Goodenough, Journal of the Electrochemical Society 144 (1997) 1188–1194.
[19] A.K. Padhi, K.S. Nanjundaswamy, C. Masquelier, S. Okada, J.B. Goodenough, Journal of the Electrochemical Society 144 (1997) 1609–1613.